HEAT AND MASS TRANSFER OF OILS IN BAFFLED AND FINNED DUCTS

by

Younes MENNI[a], Houari AMEUR[b], Ali J. CHAMKHA[c], Mustafa INC[d,e*], and Bandar ALMOHSEN[f]

[a] Unit of Research on Materials and Renewable Energies, Department of Physics, Faculty of Sciences, Abou Bekr Belkaid University, Tlemcen, Algeria
[b] Department of Technology, University Centre of Naama - Salhi Ahmed, Naama, Algeria
[c] Mechanical Engineering Department, Prince Sultan Endowment for Energy and Environment, Prince Mohammad Bin Fahd University, Al-Khobar, Saudi Arabia
[d] Department of Mathematics, Science Faculty, Firat University, Elazig, Turkey
[e] Department of Medical Research, China Medical University Hospital, China Medical University, Taichung, Taiwan
[f] Department of Mathematics, College of Science, King Saud University, Riyadh, Saudi Arabia

Original scientific paper
https://doi.org/10.2298/TSCI20S1267M

This analysis intends to simulate the forced-convection and oil flow characteristics in the turbulent regime (Re = 5000-25000) through rectangular-shaped ducts with staggered, transverse, solid, and flat baffle plates. The study is achieved by using a calculation software based on the finite volume method (FLUENT) with selected SIMPLE, Quick, and k-ε model. Two various models of baffled ducts are simulated in this analysis under steady flow conditions. In the first model (Case A), a duct with one upper fin and two lower baffles is examined. However and in the second model (Case B), a duct with two upper fins and one lower baffle is treated. The contour plots of stream-function, number of Nusselt, and coefficient of skin friction are addressed. As expected, the heat transfer rates raised in the second case (Case B), due to the presence of the lower second obstacle that directs the entire oil current towards the hot upper part of the second duct at very high velocities, resulting thus in enhanced heat transfer rates, especially in the case of high Reynolds number values.

Key words*: baffling technique, oil flow, heat exchanger duct, solar collector duct, stream-function, heat and mass transfer, heat transfer enhancement, temperature, friction coefficient, numerical simulation*

Introduction

Due to the importance of the existence of heat transfer ducts in various fields and applications, it became necessary to search for ways to increase their effectiveness. As well-known, the baffling way has been followed by many researchers, in particular in the field of solar energy, to improve the efficiency of solar receivers, or in the area of mechanics to enhance the performance of heat exchangers. Recent studies have been incorporated for different forms of obstacles, under multiple flow conditions and with distinct physical properties. Singh *et al.*

[*] Corresponding author, e-mail: minc@firat.edu.tr

[1] simulated a duct with discrete ribs of V-form. The authors investigated the impact of some structural parameters of V-ribs, *i. e.*, size, attack angle, station, spacing, and width of the gap. Sethi *et al.* [2] conducted an analysis of air-flow with heat transfer in a solar heater using an experimental model. This heater has channels roughened with dimples on their hot surfaces. The investigators examined the heat and fluid characterization in the case of variation of Reynolds number, arc angle, as well as relative height and pitch of roughness. Kumar *et al.* [3] presented studies on the heat transfer for air-flows inside a solar heater with a roughness of discrete double V-form. This experimental work reported the impact of geometrical parameters of roughness on the solar heater performance. Skullong *et al.* [4] characterized the thermal-air behavior in a duct of a heater of solar energy. The pipe considered was fitted with grooves in its wavy geometry and winglets on its absorber. They addressed the impacts of structural parameters of grooves and winglets on the thermal-air behavior inside the channel. Abene *et al.* [5] conducted studies on the evaluation of the energetical performance of a collector of solar energy. This collector has obstacles of various form configurations. The results of this collector were also compared with those obtained in the case with no attachments. Bekele *et al.* [6] experimentally presented an analysis of the thermal and aerodynamical behavior through a rectangular conduit fitted with obstacles in the delta form. The impact of variation of some structural parameters of this obstacle geometry, such as longitudinal spacing and size, for different Reynolds number has been addressed. Handoyo *et al.* [7] performed analyses on thermal-aerodynamical behavior inside an air V-waved pipe of a heater of solar energy. This pipe has obstacles with different distances of separation. Peng *et al.* [8] showed a new configuration of the air-flow collector of solar energy. The surface of its absorber has pin-fins to enhance its thermal performance. Kumar *et al.* [9] analyzed the impact of the variation of structural values of V-form obstacles in their discretized broken configuration, *i. e.*, V-geometry attack angle, size and height, the width of V-configuration gap, as well as the distance between the gap and obstacle, on the coefficients of thermal transfer and skin-friction, through an air pipe of solar energy. Kumar and Kim [10] presented a review study on the effects of attachments, such as obstacles, on the solar pipes performances. Promvonge *et al.* [11] numerically showed the performance of baffles in their inclined configuration inside a rectangular duct in 3-D. They varied the blockage ratio from 0.1-0.5 to examine its impact on heat transport and pressure loss. They also compared this situation with the case of a vertical obstacle. Mokhtari *et al.* [12] used the method of finite volumes to simulate the mixed heat convection in a 3-D pipe with different locations of fins. Mousavi and Hooman [13] reported the convective heat transfer and the control of a laminar type flow in the inlet section of a 2-D duct with obstacles on their walls. Yongsiri *et al.* [14] showed numerical data on the heat transfer for turbulent flows through a pipe provided by inclined ribs with detached geometries. Karwa and Maheshwari [15] studied two different cases of perforated obstacles, fully/half perforation. Kamali and Binesh [16] simulated the thermal-aerodynamical behavior inside a square conduit with ribs of different geometrical types placed on one surface. Some other outstanding contributions can be found in [17-20]. The authors simulated fluid-flow and heat transfer under different conditions.

The completed studies, listed previously, have shown that inserting the obstacles improves the channel performance because the technique creates spaces with very high temperatures. However, most of these studies relied on air for heat transfer. This fluid has low physical properties; that is, its thermal conductivity is very low. From this viewpoint, this work shows the characteristics of heat transfer and oil mass of two different horizontal rectangular ducts fitted with three staggered obstacles attached to the hot upper and insulated lower opposite walls. The study is achieved under turbulent flow conditions.

Computational domain

In the present paper, a 2-D comparison between two different ducts equipped with fins and baffle plates is performed. The two proposed geometrical configurations, which are indicated as Cases A and B, are shown in fig. 1, as well as, all essential elements, such as geometric dimensions and limit parameters, are also illustrated in fig. 1.

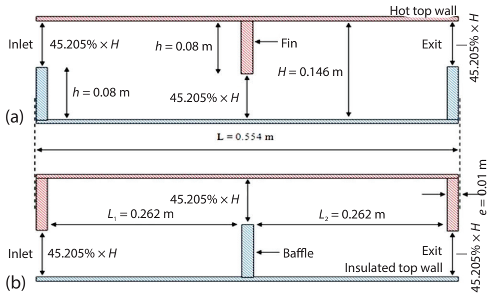

Figure 1. The different geometrical configurations under analysis; (a) type A, and (b) type B

Both A and B geometrical models are investigated and compared according to the following physical assumptions and hydrothermal boundary conditions:

– The thermal-physical characteristics of oil fluid and Al solid are constant. They are reported in [21, 22].
– The oil flow is assumed to be incompressible, turbulent (Re = 5000-25000) and steady.
– A uniform 1-D profile of intake velocity, $u = U_{in}$ is employed [23, 24].
– The oil temperature, T_{in}, is 298 K at the duct intake [22].
– The temperature of the lower surface in the upper wall of the duct is constant, T_w = 375 K [23].
– The lower wall of this same duct is insulated.
– The atmospheric pressure, P_{atm}, is applied at the exit section of the duct [24].
– Impermeable boundary and no-slip wall conditions are applied for the solid surfaces.
– The forced-convection type transfer of heat is considered, while the thermal transfer by radiation is neglected.
– The following geometry parameters, the length and height of the ducts (L = 0.554 m and H = 0.146 m), as well as the height of the obstacles (h = 0.08 m) were approved from the numerical and experimental analysis of Demartini and his colleagues in [24].

The present work is a complementary analysis of our previous studies, referenced in [25, 26]. A detailed analysis of the velocity fields and their curves at different locations from the ducts is included in the referenced paper [25]. While, the dynamic pressure, turbulent kinetic energy, as well as turbulent viscosity contours are discussed in the second part of the work [26].

Modelling and simulation

The equations of conservation, *i. e.*, continuity, momentum and energy, that are governing the hydrothermal characteristics of oil flow in these newly geometrical models, are presented:

Continuity equation [24]:

$$\frac{\partial u_j}{\partial x_j} = 0 \tag{1}$$

Momentum equation [24]:

$$\rho u_j \frac{\partial u_i}{\partial x_j} = -\frac{\partial P}{\partial x_i} + \frac{\partial}{\partial x_j}\left(\mu \frac{\partial u_i}{\partial x_j} - \rho \overline{u_i' u_j'}\right) \tag{2}$$

where, ρ is the density of the fluid, P – the pressure, μ – the dynamic viscosity, u_i and u_j are mean velocity components in x_i- and x_j-directions, u'_i and u'_j – fluctuation velocity components in x_i and x_j directions, with [24]:

$$-\rho\overline{u'_i u'_j} = \mu_\mathrm{t}\left(\frac{\partial u_i}{\partial x_j}+\frac{\partial u_j}{\partial x_i}\right)-\frac{2}{3}\rho\delta_{ij}k \tag{2a}$$

$$\mu_\mathrm{t} = \rho C_\mu \frac{k^2}{\varepsilon} \tag{2b}$$

Energy equation:

$$\rho u_j \frac{\partial T}{\partial x_j} = \frac{\partial}{\partial x_j}\left[\left(\frac{\mu}{\mathrm{Pr}}+\frac{\mu_\mathrm{t}}{\mathrm{Pr}_\mathrm{t}}\right)\frac{\partial T}{\partial x_j}\right] \tag{3}$$

where μ_t is the turbulent viscosity, and δ_{ij} is the Kroenecker delta.

Turb-kinetic-energy, k, [27]:

$$\rho u_j \frac{\partial k}{\partial x_j} = \frac{\partial}{\partial x_j}\left[\left(\mu+\frac{\mu_\mathrm{t}}{\sigma_k}\right)\frac{\partial k}{\partial x_j}\right]+G_k-\rho\varepsilon \tag{4}$$

Turbulence dissipation rate, ε [27]:

$$\rho u_j \frac{\partial \varepsilon}{\partial x_j} = \frac{\partial}{\partial x_j}\left[\left(\mu+\frac{\mu_\mathrm{t}}{\sigma_\varepsilon}\right)\frac{\partial \varepsilon}{\partial x_j}\right]+C_{1\varepsilon}\frac{\varepsilon}{k}G_k-C_{2\varepsilon}\rho\frac{\varepsilon^2}{k} \tag{5}$$

where $C_\mu = 0.09$, $C_{1\varepsilon} = 1.44$, $C_{2\varepsilon} = 1.92$, $\sigma_k = 1.0$, and $\sigma_\varepsilon = 1.3$ are the constants of the turbulence model [27]. The mesh is structural quadrilateral non-uniform 2-D and refined at all solid boundaries. The finite volume method [28], the *SIMPLE* algorithm (semi implicit method for pressure linked equations) [28], the *QUICK* scheme (quadratic upstream interpolation for convective kinetics) [29], as well as the (standard) k-ε model [27] are used to model the heat and oil mass transfer, and the FLUENT software are employed for this analysis. The effect of mesh density on the numerical solution, as well as the validity of the used numerical model are detailed in the first part of this work, which is presented in [25].

Results and discussion

The evolution of the oil flow is visualized in both Cases A and B by showing the distribution of streamlines inside the baffled and finned ducts, fig. 2. It is apparent that the flow field is unstable due to the presence of the obstacles. From the figure, the flow path is wavy in both ducts, which gives an irregular flow structure.

This structure is very complex, characterized by the presence of direct currents, flowing from the left to right at high speeds, especially in the regions adjacent to the edges of the baffles and fins, where the dynamic pressure values rise due to a decrease in the hydraulic diameter of the ducts.

As expected, the reduction in dynamic pressure values, on the front sides of the deflectors, results in a detachment of the flow field on the front top sharp edges of the obstacles, leading to the formation of recycling cells on their front and back sides. These vortices are very intense next to the right sides of the first and second obstacles. The intensity, strength, and extension of these re-circulation cells increase with augmenting numbers of Reynolds, especially in the following areas of the first and second obstacles, in the Cases B and A, respectively. Consequently, the obstacles affect the hydrodynamic characteristics of the oil flow by changing its path and secreting secondary currents in the form of vortices, in both types A and B.

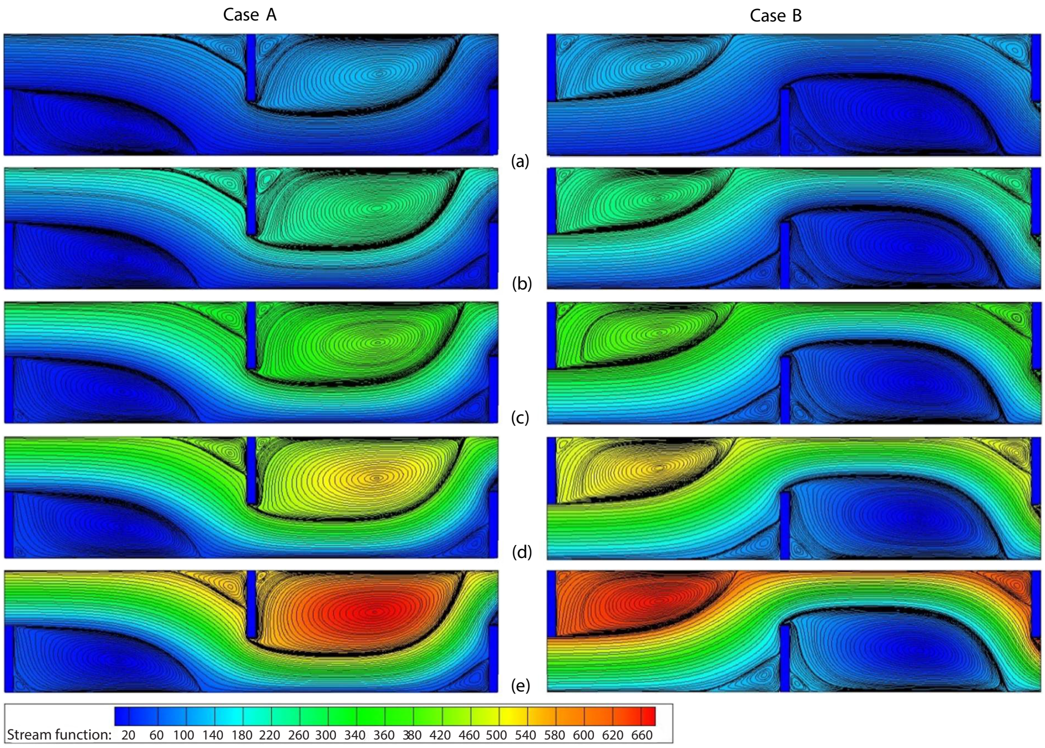

Figure 2. Stream function, Ψ [kgs^{-1}], fields for Cases A and B; (a) Re = 5000, (b) Re = 10000, (c) Re = 15000, (d) Re = 20000, and (e) Re = 25000

Figure 3 shows the maximum Ψ values for the two studied cases. For the range of Reynolds number from 5000-5000, it appears that the finned-line alignment model in the first Case A contributes to higher stream-function values, compared to the second model. However, in the latter Case B, there is ample space for flowing near the hot upper side of the duct, which raises the heat transfer between the hot surface and the oil fluid.

The axial evolution of the local number of Nusselt, Nu_x, along the hot wall in both studied Cases A and B is reported in fig. 4. In the first Case A, the Nu_x values are very high at the duct entrance section, due to the flow of current from the upper part adjacent to its hot surface,

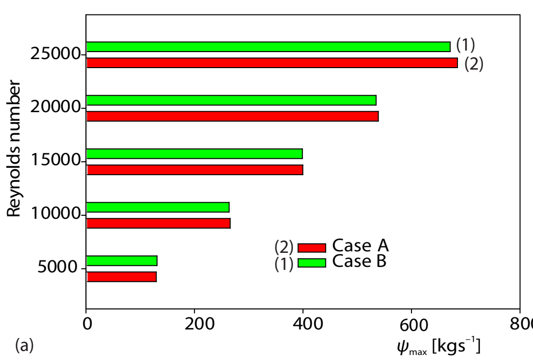

Figure 3. The Ψ_{max} values for various Reynolds numbers in both Cases A and B

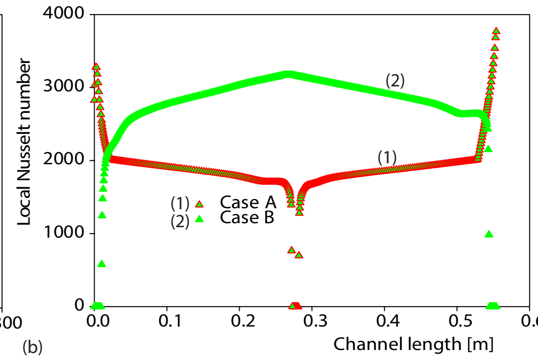

Figure 4. The Nu_x profiles along the hot channel surface for both models A and B, Re = 5,000

and also at its exit, due to the presence of the last third obstacle attached on the thermally insulated wall that directs the current towards the hot top wall with high velocities. Conversely, the local Nusselt number is decreasing next to the left and right sides of the upper second obstacle, as a result of the variation in the flow direction, from the top to lower parts of the duct.

For the second studied Case B, the Nu_x values are very high in the vicinity of the upper face of the second obstacle, fig. 4. This improvement in heat transfer is due to three main factors:

– The first factor is the presence of a strong recycling cell, next to the right side of the first obstacle, near the hot upper wall to the left of the second obstacle.
– The second factor is the presence of the lower second obstacle, which drives the current over its sharp top edge, towards the hot duct part, at high velocities and intense frictions, thus an excellent heat transfer.
– The third factor is the presence of the massive vortex at the lower part of the duct, behind the second obstacle. At the end of the canal, the Nu_x values decrease directly, resulting thus in a change of the direction of the current towards the duct output at its bottom part.

On the other hand, the heat transfer coefficients in terms of local Nusselt numbers can be enhanced by augmenting the Reynolds number value in both Cases A and B. As shown in figs. 5(a) and 5(b), there is a positive relationship between the augmetation in Reynolds number values and the improvement in Nu_x values. For the same range of Reynolds number number considered here, *i. e.*, from 5000-25000, there is also an improvement in the heat transfer, in terms of average Nusselt numbers, and this for all the cases investigated. The duct structure according to the second model, *i. e.*, type B, promotes better heat transfer compared to the configuration of the first type A, due to the high temperature gradients that occupy the majority of the upper wall, especially next to the top gap due to the presence of the lower second obstacle, fig. 6. At the lowest value of Reynolds number, *i. e.*, 5000, the amount of Nusselt number is about 222.48 in the latter Case B. This value drops by about 31% in the first Case A. on the other hand, the number of Nu exceeds the amount of 400 in the second model, at the maximum Reynolds number value, *i. e.*, there is an increase of 6% compared to the first model at the same maximum amount of Reynolds number. Moreover, the heat transfer enhancement is improved by 151% in the first type, while by 82% when the Reynolds number changes from 5000-25000.

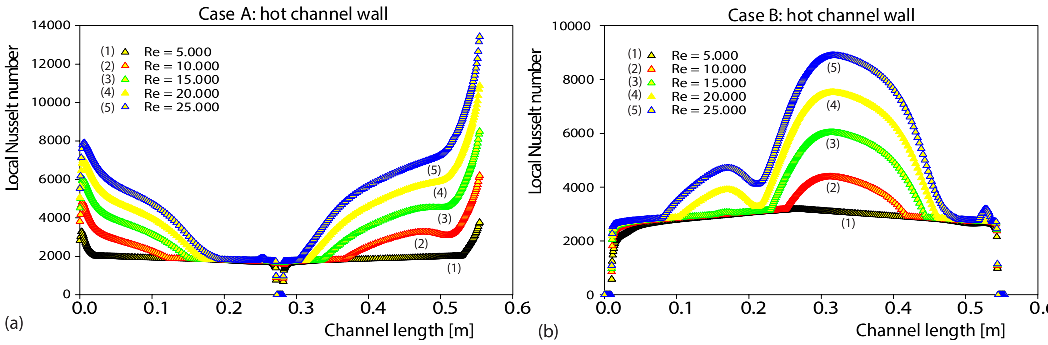

Figure 5. Effect of Reynolds number on Nu_x profiles for (a) Case A and (b) Case B

The skin friction coefficient values, C_f, are very low on the left and right sides of the upper second obstacle, fig. 7. The C_f values are slightly increased in the back region of the same obstacle, due to the presence of a strong recycling cell near its right side. Then, C_f decreases until it reaches its minimum value at the separation point between the end of the recy-

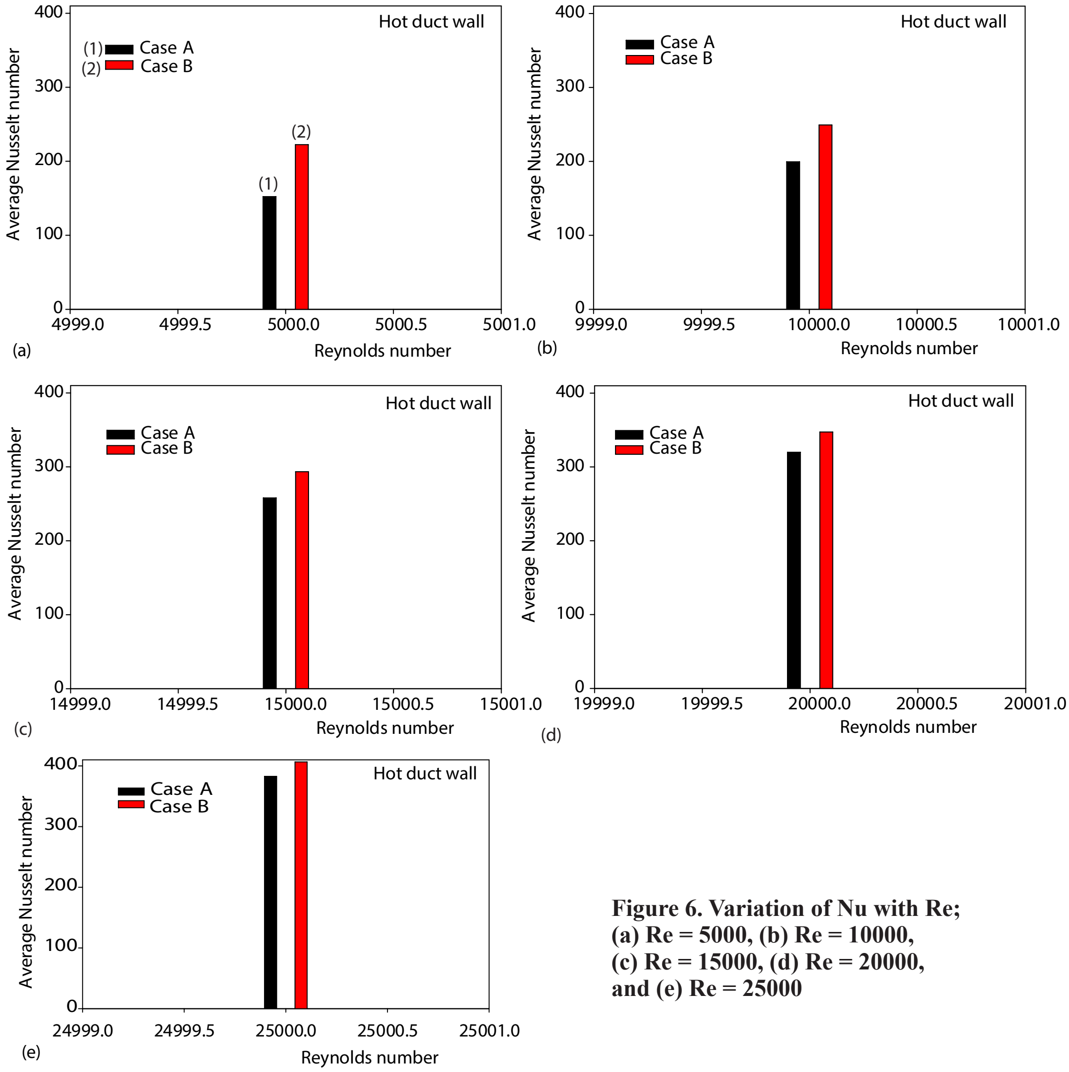

Figure 6. Variation of Nu with Re; (a) Re = 5000, (b) Re = 10000, (c) Re = 15000, (d) Re = 20000, and (e) Re = 25000

cling cell extension and the contact start of the mainstream with the hot surface of the duct. In contrast, the C_f values are very high at the end of the canal, due to the significant change in the flow direction from the bottom part of the duct to the upper part towards its exit from the last third obstacle. These notes are valid for the first Case A, as shown in fig. 7.

In the second Case B studied, the second obstacle is mounted on the thermally insulated bottom wall. The presence of this obstacle allows the entire flow to be directed towards the hot top part, where the pressure and velocity

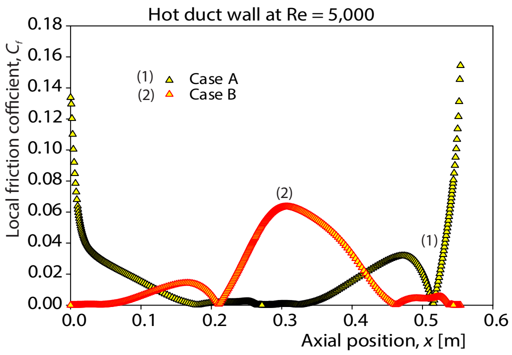

Figure 7. The C_f profiles along the hot duct wall, for both Cases A and B and Re = 5000

increase through the gap adjacent to its sharp upper edge and thus, the C_f values increase with the hot surface adjacent to the tip of this obstacle. The C_f values are also high next to the right side of the same obstacle, due to a strong re-circulation zone in this region. This re-circulation drives the main flow at its upper end toward the upper hot space of the duct. The C_f values are slightly elevated after the first obstacle, due to the presence of a recycling cell on the backside of the same obstacle. The friction values decrease near the left side of the last third obstacle, resulting thus in a decrease of the pressure, and the flow is directed towards the outlet of the duct in its lower part, fig. 7.

Conclusions

The following main observations can be made.

- Noticeable vortices are formed next to the right sides of the first and second obstacles in both Cases A and B studied. The strength and extension of these cells of re-circulation increase with increasing Reynolds number values, especially on the following areas of the first and second obstacles in Cases B and A, respectively.
- The internal structure of the first pipe (Case A) helps to create powerful cells for recycling compared to the second pipe (Case B), and this for all the Reynolds number values followed.
- The duct structure according to the second model, *i. e.*, type (B), promotes better heat transfer compared to the configuration of the first type (A), due to the high temperature gradients that occupy the majority of the upper wall, especially next to the top gap, due to the presence of the lower second obstacle.
- At the lowest value of Reynolds number, *i. e.*, 5000, the amount of Nusselt number is about 222.48 in the second Case B. This value drops by about 31% in the first Case A.
- The number of Nusselt number exceeds the value of 400 in the second model (B), at the maximum Reynolds number value, *i. e.*, there is an increase of 6% compared to the first model (A) at the same maximum amount of Reynolds number.
- The heat transfer enhancement in terms of average Nusselt number is improved by 151% in the first duct type, while by 82% when the Reynolds number changes from 5000-25000.

Nomenclature

C_f – skin friction coefficient, [–]
$C_{1\varepsilon}$ – k-ε model constant, [–]
$C_{2\varepsilon}$ – k-ε model constant, [–]
$C_{3\varepsilon}$ – k-ε model constant, [–]
C_μ – k-ε model constant, [–]
h – baffle and fin height, [m]
H – duct height, [m]
k – turbulent kinetic energy, [m^{-2}s^{-2}]
L – duct length, [m]
L_1 – first-second obstacles' distance, [m]
L_2 – second-third obstacles' distance, [m]
Nu_x – local Nusselt number, [–]
Nu – average Nusselt number, [–]
P – pressure, [Pa]
P_{atm} – atmospheric pressure, [Pa]
Pr – Prandtl number, [–]
Re – Reynolds number, [–]
T – temperature, [K]
T_{in} – inlet temperature, [K]
T_{w} – Wall temperature, [K]
u_i – velocity component in x_i-direction, [ms^{-1}]
U_{in} – inlet velocity, [ms^{-1}]
u_j – velocity component in x_i direction, [ms^{-1}]

Greek symbols

δ_{ij} – Kroenecker delta, [–]
ε – turbulent dissipation rate, [m^{2}s^{-3}]
μ – dynamic viscosity, [kgm^{-1}s^{-1}]
μ_t – turbulent viscosity, [kgm^{-1}s^{-1}]
ρ – fluid density, [kgm^{-3}]
σ_k – k-ε model constant, [–]
σ_ε – k-ε model constant, [–]
Ψ – stream-function, [kgs^{-1}]

Subscripts

atm – atmospheric
in – inlet
max – maximum
k – for k-equation
t – turbulent
w – wall
ε – for ε-equation

Acknowledgment

B. Almohsen is supported by Researchers Supporting Project number (RSP-2020/158), King Saud University, Riyadh, Saudi Arabia.

Reference

[1] Singh, S., *et al.*, Heat Transfer and Friction Factor Correlations of Solar Air Heater Ducts Artificially Roughened with Discrete V-Down Ribs, *Energy*, *36* (2011), 8, pp. 5053-5064
[2] Sethi, M., *et al.*, Correlations for Solar Air Heater Duct with Dimpled Shape Roughness Elements on Absorber Plate, *Solar Energy*, *86* (2012), 9, pp. 2852-2861
[3] Kumar, A., *et al.*, Heat Transfer and Friction Correlations for Artificially Roughened Solar Air Heater Duct with Discrete W-Shaped Ribs, *Energy Conversion and Management*, *50* (2009), 8, pp. 2106-2117
[4] Skullong, S., *et al.*, Heat Transfer Augmentation in a Solar Air Heater Channel with Combined Winglets and Wavy Grooves on Absorber Plate, *Applied Thermal Engineering*, *122* (2017), July, pp. 268-284
[5] Abene, A., *et al.*, Study of a Solar Air Flat Plate Collector: Use of Obstacles and Application for the Drying of Grape, *Journal of Food Engineering*, *65* (2004), 1, pp. 15-22
[6] Bekele, A., *et al.*, Effects of Delta-Shaped Obstacles on the Thermal Performance of Solar Air Heater, *Advances in Mechanical Engineering*, *2011* (2011), 103502
[7] Handoyo, E. A., *et al.*, Numerical Studies on the Effect of Delta-Shaped Obstacles' Spacing on the Heat Transfer and Pressure Drop in V-Corrugated Channel of Solar Air Heater, *Solar Energy*, *131* (2016), June, pp. 47-60
[8] Peng, D., *et al.*, Performance Study of a Novel Solar Air Collector, *Applied Thermal Engineering*, *30* (2010), 16, pp. 2594-2601
[9] Kumar, R., *et al.*, Experimental Study and Correlation Development for Nusselt Number and Friction Factor for Discretized Broken V-Pattern Baffle Solar Air Channel, *Experimental Thermal and Fluid Science*, *81* (2017), Feb., pp. 56-75
[10] Kumar, A., Kim, M. H., Convective Heat Transfer Enhancement in Solar Air Channels, *Applied Thermal Engineering*, *89* (2015), Oct., pp. 239-261
[11] Promvonge, P., *et al.*, Numerical Investigation of Laminar Heat Transfer in a Square Channel with 45° Inclined Baffles, *International Communications in Heat and Mass Transfer*, *37* (2010), 2, pp. 170-177
[12] Mokhtari, M., *et al.*, Numerical Study of Mixed Convection Heat Transfer of Various Fin Arrangements in a Horizontal Channel, *Engineering Science and Technology*, *20* (2017), 3, pp. 1106-1114
[13] Mousavi, S. S., Hooman, K., Heat and Fluid-Flow in Entrance Region of a Channel with Staggered Baffles, *Energy Conversion and Management*, *47* (2006), 15-16, pp. 2011-2019
[14] Yongsiri, K., *et al.*, Augmented Heat Transfer in a Turbulent Channel Flow with Inclined Detached-Ribs, *Case Studies in Thermal Engineering*, *3* (2014), July, pp. 1-10
[15] Karwa, R., Maheshwari, B. K., Heat Transfer and Friction in an Asymmetrically Heated Rectangular Duct with Half and Fully Perforated Baffles at Different Pitches, *International Communications in Heat and Mass Transfer*, *36* (2009), 3, pp. 264-268
[16] Kamali, R., Binesh, A. R., The Importance of Rib Shape Effects on the Local Heat Transfer and Flow Friction Characteristics of Square Ducts with Ribbed Internal Surfaces, *International Communications in Heat and Mass Transfer, 35* (2008), 8, pp. 1032-1040
[17] Yu, C., *et al.*, Numerical Study on Turbulent Heat Transfer Performance of a New Compound Parallel Flow Shell and Tube Heat Exchanger with Longitudinal Vortex Generator, *Applied Thermal Engineering*, *164* (2020), 114449
[18] Nakhchi, M. E., *et al.*, Numerical Study of Turbulent Flow Inside Heat Exchangers Using Perforated Louvered Strip Inserts, *International Journal of Heat and Mass Transfer*, *148* (2020), 119143
[19] Lv, J. Y., *et al.*, Active Design for the Tube Insert of Center-Connected Deflectors Based on the Principle of Exergy Destruction Minimization, *International Journal of Heat and Mass Transfer*, *150* (2020), 119260
[20] Nidhul, K., Enhanced Thermo-Hydraulic Performance in a V-Ribbed Triangular Duct Solar Air Heater: CFD and Exergy Analysis, *Energy*, *200* (2020), 117448
[21] Derakhshan, M. M., Akhavan-Behabadi M. A., Mixed Convection of MWCNT Heat Transfer Oil Nanofluid inside Inclined Plain and Microfin Tubes under Laminar Assisted Flow, *International Journal of Thermal Sciences*, *99* (2016), Jan., pp. 1-8

[22] Gholami, M. R. *et al.*, The Effect of Rib Shape on the Behavior of Laminar Flow of Oil/MWCNT Nanofluid in a Rectangular Micro-Channel, *Journal of Thermal Analysis and Calorimetry*, *134* (2018), 3, pp. 1611-1628
[23] Nasiruddin, Kamran Siddiqui, M. H., Heat Transfer Augmentation in a Heat Exchanger Tube Using a Baffle, *International Journal of Heat and Fluid-flow*, *28* (2007), 2, pp. 318-328
[24] Demartini, L. C., *et al.*, Numeric and Experimental Analysis of the Turbulent Flow through a Channel with Baffle Plates, *Journal of the Brazilian Society of Mechanical Sciences and Engineering*, *26* (2004), 2, pp. 153-159
[25] Menni, Y., *et al.*, Hydrodynamic Behavior in Solar Oil Heat Exchanger Ducts Fitted with Staggered Baffles and Fins, *Journal of Applied and Computational Mechanics*, 2020,
[26] Menni, Y., *et al.*, Numerical Simulation of Dynamic Pressure and Kinetic Energy Fields of Turbulent Oil Flow in Staggered Baffled Pipes, *Mathematical Modelling of Engineering Problems*, *7* (2020), 1, pp. 10-16
[27] Launder, B. E., Spalding, D. B., The Numerical Computation of Turbulent Flow, *Computer Methods in Applied Mechanics and Engineering*, *3* (1974), 2, pp. 269-289
[28] Patankar, S. V., *Numerical Heat Transfer andFluid-flow*, McGraw-Hill, New York, USA, 1980
[29] Leonard, B. P., Mokhtari, S., Ultra-Sharp Non-Oscillatory Convection Schemes for High-Speed Steady Multidimensional Flow, NASA TM 1-2568, NASA Lewis Research Center, Cleveland, O., USA, 1990

Paper submitted: April 25, 2020
Paper revised: June 10, 2020
Paper accepted: June 20, 2020